Proceedings of GPPS Forum 18
Global Power and Propulsion Society
Montreal, 7th-9th May 2018
www.gpps.global

GPPS-2018-0012

EXPERIMENTAL ANALYSIS OF THE FUEL FLEXIBILITY OF A JET-STABILIZED MICRO GAS TURBINE COMBUSTOR DESIGNED FOR LOW CALORIFIC GASES

Hannah E. Bower
German Aerospace Center (DLR)
Hannah.Bower@dlr.de
Stuttgart, Germany

Felix Grimm
German Aerospace Center (DLR)
Felix.Grimm@dlr.de
Stuttgart, Germany

Andreas Schwärzle
German Aerospace Center (DLR)
Andreas.Schwaerzle@dlr.de
Stuttgart, Germany

Jürgen Roth
German Aerospace Center (DLR)
Juergen.Roth@dlr.de
Stuttgart, Germany

Timo Zornek
German Aerospace Center (DLR)
Timo.Zornek@dlr.de
Stuttgart, Germany

Peter Kutne
German Aerospace Center (DLR)
Peter.Kutne@dlr.de
Stuttgart, Germany

ABSTRACT

Fuel flexible burners are an important concept to aid in the advancement and implementation of renewable energy sources into existing infrastructure. As focus shifts from conventional to renewable fuel sources, designing gas turbines which meet both the technical and load requirements for fluctuating fuel compositions and heating values is imperative. The present work aims to study the stability and fuel flexibility of a two-stage burner, consisting of a jet-stabilized main stage and a swirl-stabilized pilot stage. Various fuel compositions, consisting of natural gas, hydrogen, carbon monoxide, carbon dioxide and nitrogen, with lower heating values ranging from 7MJ/kg to 49MJ/kg at an air preheat temperature of 873K were tested. Additionally, differing power loads (60kW to 100kW) and air-fuel equivalence ratio ranges (1.5-3.6) were examined. This study utilized OH* chemiluminescence measurements in conjunction with exhaust gas analysis of carbon monoxide and nitrogen oxide levels to assess the operation and reliability of the burner. Moreover, the experimental results are supported by steady state computational fluid dynamics simulations to provide explanation of the flame flow field characteristics and kinetics. The results indicate flame stability and low emissions levels for the majority of fuel compositions and thermal loads tested, therefore signifying high fuel flexibility of the burner. Additionally, optimal combustor operating points, which display emissions levels below the proposed German legal limits (German Federal Ministry for the Environment, 2016), were determined. Furthermore, the computational fluid dynamics simulation results indicate a good match to the experimental results, providing insight into the burner flow field characteristics and kinetics.

INTRODUCTION

Micro gas turbines (MGTs) for combined heat and power are a promising technology that offers many advantages for small-scale power generation, including the potential to curb increases in emissions (Palavachi, 2002). Additionally, the ability of MGTs to produce a stable flame allows for the flexibility to use alternative fuels (Gupta et al., 2010). As many countries focus on increasing the amounts of energy produced via renewable resources, technologies that ease the transition from traditional to alternative energy sources, while still providing grid stability and supply safety, are important. Therefore, fuel flexible burners are an important concept to aid in the advancement and implementation of renewable energy sources into existing infrastructure.

Swirl stabilized burners are currently used in gas turbines, where swirling air generates toroidal recirculation zones, stabilizing the (main stage) flame (Huang and Yang, 2009). However, as swirl stabilized burners in MGTs operate at lean premixed conditions (LPCs), to achieve adequate efficiencies and reasonable emissions levels, LPCs also stimulate thermo-acoustic instabilities (Huang and Yang, 2009). The thermo-acoustic instabilities negatively influence the combustion reactions, which increase the exhaust gas emissions levels (Zanger et al., 2015). Therefore, flameless oxidation (FLOX®) burners are currently being developed to

operate steadily and produce low emissions levels at all MGT load points. For example, a two-stage FLOX®-based combustion system was recently designed and tested using natural gas fuel in a Turbec T100PH Series 3 MGT, with an electrical power output of 100kW and an electrical efficiency of approximately 30% (Zanger et al., 2015). The combustor displayed CO exhaust gas emissions levels below that of a standard Turbec T100 combustor for two burner configurations tested. Furthermore, the NO_x emissions levels were well below the current German legal limit (German Federal Ministry for the Environment, 2002), signifying a feasible (two-stage Turbec T100) combustion system (Zanger et al., 2015).

While natural gas is one of the most commonly used fuel types for MGT combustors, as it is easily accessible via the current infrastructure and has high combustibility, syngas produced from biomass is an efficient and technically viable fuel source for reducing emissions levels. There are two pathways for the production of power from woody biomass: combustion and gasification (Spliethoff, 2010). In the gasification process, syngas fuel is produced at air-deficient conditions via the addition of air or another gasification agent, such as water vapor (Spliethoff, 2010). Two-stage MGT combustors, adopted from the FLOX® principle, using syngas fuel, with lower heating values (LHVs) between 2.5MJ/kg and 5MJ/kg, have been successfully operated in a Turbec T100, producing electrical power outputs between 50-100 kW (Zornek et al., 2015). The MGT combustor system produced CO and NO_x emissions levels less than 30ppm and 6ppm, respectively (Zornek et al., 2015).

Although syngas is a viable fuel source for MGTs, the energy supply from the gasification process is not always reliable. Unreliability from the gasification process can be due to logistical and technical problems, from the collection of biomass to electricity generation (Asadullah, 2014), including varying biomass quality, impurities in the fuel gas and fluctuations during the gasification process. Therefore, the ability to switch between natural gas and syngas, without degrading the power plant stability or having to change the MGT electronics and mechanical infrastructure, is of high importance.

The present work focuses on the experimental testing of a previously studied two-stage burner, adopted from the FLOX® principle, designed for use with syngas fuel produced by biomass gasification (Zornek et al., 2013; Zornek et al., 2015). In this study, the existing burner, in an optically accessible atmospheric test rig, using various natural gas and syngas fuel mixtures, is studied to determine the stability and fuel flexibility of the combustor system. The exhaust gas is analyzed for CO and NO_x emissions and OH* chemiluminescence measurements are performed to examine the location and shape of the heat release zones. Moreover, the experimental results are supported by steady state computational fluid dynamics (CFD) simulations, using detailed reaction models for explanation of the flow field characteristics and kinetics.

METHODOLOGY

The combustor presented in this paper was installed and tested in an atmospheric test rig, with gas analysis and OH* chemiluminescence systems used for data acquisition and examination. Furthermore, a test matrix was constructed and used to test a range of variables at steady state operating conditions. Lastly, CFD simulations of the combustor system were performed using a detailed chemistry model.

Atmospheric Test Rig and Data Acquisition Equipment

The experimental test rig consists of a fuel transport system, air preheat system and combustor system. Figure 1 depicts the combustor system and experimental setup. The combustor system setup consists of a burner, with ten jet-stabilized main stage nozzles arranged in an annular configuration, a swirl stabilized pilot stage and a main air inlet. Preheated air enters the air plenum and impinges a baffle, which guides the air flow. The air is then homogenized via an additional perforated plate and is redirected 180° before splitting between the main stage and the pilot stage. The test rig also consists of an optically accessible combustor top, consisting of six quartz glass windows and an upper flange with an exhaust cap. The upper flange further secures the windows into place and allows for an exhaust gas probe to enter the combustion chamber. Furthermore, the high speed camera system is mounted approximately one meter from the combustor system to provide adequate space for the focusing of the UV objective and for heat dissipation of the combustion chamber.

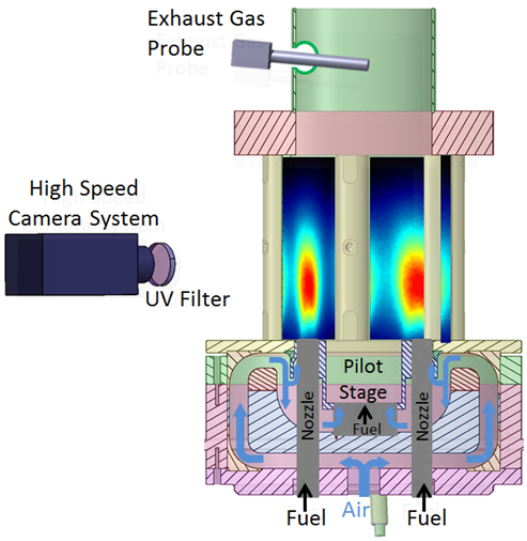

Figure 1 Combustor System and Data Acquisition Setup Schematic

The stability and fuel flexibility of the combustor system was determined by OH* chemiluminescence and exhaust gas measurements. OH* chemiluminescence is a commonly used technique to investigate the physical characteristics of a flame (Schütz et al., 2006; Lückerath et al., 2007; Zanger et al., 2011). For this technique, excited hydroxyl radicals

(OH*) are produced during the combustion reaction, which then transition from an excited atomic energy state to a lower atomic energy state and emit light at a wavelength of approximately 309nm (Kathrotia, 2011). Since the hydroxyl radical is only present in the excited state for a short period of time, capturing the light released from the energy state transition is a good indicator of the flame reaction zone characteristics. Figure 2 depicts the OH* chemiluminescence field of view.

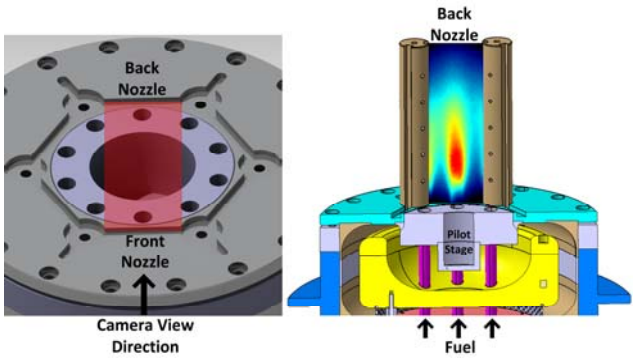

Figure 2 OH* Chemiluminescence Field of View Schematics

In the present work, a LaVision High Speed Star charge coupled device (CCD) camera, equipped with a High Speed Intensified Relay Optics (IRO) intensifier, a CERCO 100mm F/2.8 UV lens and a UV interference filter ($\lambda = 312 \pm 20$nm) were used to capture the OH* chemiluminescence at a sampling rate of 100Hz . The IRO was kept at a gain of 30000µs and a gate of 75% throughout the experiments. Additionally, 500 line of sight integrated images were captured and processed by LaVision DaVis software and in-house scripts. The background and sensitivity field were first subtracted and divided out of each image, respectively. The images were then averaged and the intensity was normalized to both a global maximum and an individual image maximum. Lastly, the lift-off height was calculated by determining the flame region (pixels with intensities at or above 50% of the maximum intensity present in the image) and averaging the height of the boundary pixels in the bottom 30% of the flame region.

Exhaust gas measurements were also taken via an ABB process gas analyzer (Advanced Optima Process Gas Analyzer AO2000) and assessed using an in house script. The gas samples were extracted from the combustion chamber with an air cooled probe, where the flue gas was cooled to 200°C to preserve the chemical composition of the gas sample. The gas analyzer detected the H_2O, CO_2 and O_2 content, as well as the unburned hydrocarbons (UHC), carbon monoxide (CO) and nitrogen oxides (NO_x: combination of NO and NO_2 emissions) concentrations. Furthermore, the gases were measured in dry conditions and normalized to 15% O_2 content. The measurements were logged at 2Hz and time averaged over 2 minutes at steady state conditions. Table 1 displays the achievable accuracies (as absolute values) of the measured species for the given ranges.

Table 1 ABB Process Gas Analyzer (AO2000) Accuracies for the Given Species Ranges

Species	CO (ppm)	UHC (ppm)	NO_x (ppm)	O_2 (Vol.-%)	CO_2 (Vol.-%)
Range 1	0-10	0-19	0-10	0-5	0-5
Accuracy	0.1	0.37	0.1	0.025	0.05
Range 2	0-100	0-187	0-20	0-15	0-20
Accuracy	1	3.73	0.2	0.075	0.2
Range 3	0-200	0-3733	0-50	0-25	
Accuracy	2	74.7	0.5	0.0125	
Range 4	0-500	0-9322	0-200	0-100	
Accuracy	5	186.6	2.0	0.5	

Experiments

A comprehensive test matrix was constructed to provide adequate information for assessing the functionality of the burner at steady state conditions for all thermal load, air-fuel equivalence ratio (AFER) and lower heating value ranges tested. The syngas components were kept at constant volume percent ratios for all points tested, as displayed in Table 2. The volume percentages for all the syngas components are considered to be within the normal output range for a standard biomass gasifier with water vapor (Dahmen et al., 2012). Numerous syngas fuel mixtures were tested and diluted with varying amounts of natural gas (composed of approximately 92% methane), in order to test a range of lower heating values from 7MJ/kg (only syngas) to 49MJ/kg (only natural gas).

Table 2 Syngas Components and the Corresponding Volume Percentages

Syngas Component	Volume Percentage (%)
H_2	32
CO	32
CO_2	18
N_2	18

A total of 72 test points were constructed in the matrix, consisting of eight different AFER values per thermal load at each lower heating value tested, as depicted in Figure 3. The figure shows a condensed branched-tree illustration of the constructed test matrix for the assessment of the steady state combustor operating points. Only one lower heating value tested is displayed for simplicity. Take note that the red text indicates that different lower heating values were tested (49MJ/kg, 20MJ/kg, 7MJ/kg), while the remainder of the parameters examined in the tree (shown as black text) were kept consistent for all lower heating values tested. The 60kW-100kW thermal power range was normalized to atmospheric conditions and tested to cover the full Turbec T100 operating range. Additionally, the air preheat temperature remained at 873K. Moreover, approximately 7% of the air was supplied into the pilot stage and 93% was fed

into main stage of the combustor for all steady state operating points.

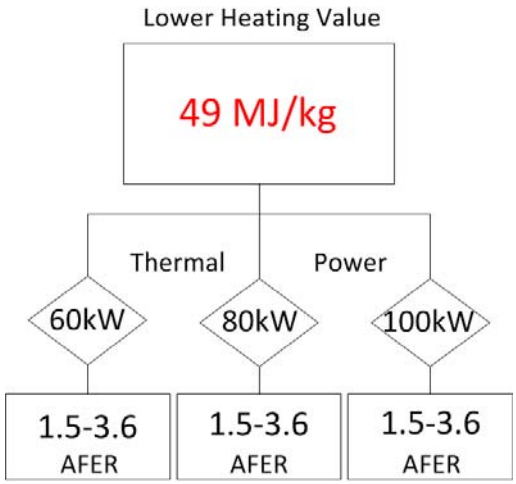

Figure 3 Branched-Tree Illustration of the Test Matrix for One Lower Heating Value Tested

CFD Simulation Setup

Computational fluid dynamics simulations were performed in order to provide insight into the flow field characteristics and chemical kinetics of the measured data. Two test cases (7MJ/kg and 49MJ/kg) were simulated via a steady state Reynolds averaged Navier Stokes (RANS) approach, with the operating conditions listed below in Table 3.

Table 3 Operating Conditions of the CFD Simulation Cases

Case	LHV (MJ/kg)	AFER (-)	Thermal Power (kW)
Methane	49	2.35	80
Syngas	7	2.35	80

The simulated domain corresponds to the same volume captured by the OH* chemiluminescence experiments (displayed in Figure 2), including the upstream air deflection. Simulations were performed using commercial ANSYS Fluent software. The computational grid was fully unstructured and consisted of 6.1 million tetrahedral cells with 1.24 million grid points. The grid was further refined in the main and pilot stage reaction zones, as well as upstream, in the fuel/air mixing sections.

The turbulence was modelled with a $k\varepsilon$-realizable approach and the reactions were depicted with an eddy dissipation concept (EDC). Furthermore, the upstream boundaries were set as the inlet mass-flows and the outlet static pressure was considered to be ambient. For the methane (49MJ/kg) test case, the DRM22 mechanism (Kazakov et al., 1994) was employed, whereas the syngas (7MJ/kg) test case was simulated with a detailed scheme presented in literature (Li et al., 2007).

RESULTS AND DISCUSSION

The results indicate flame stability and low emissions levels for the majority of fuel compositions and thermal loads tested, therefore signifying high fuel flexibility of the burner. The OH* chemiluminescence data gives a comprehensive view of the behavior of the burner at varying conditions, as well as an increased understanding of the effect of fluctuating fuel composition on the flame stability and emissions levels. Furthermore, the experimental results are supported by steady state CFD simulations, where the results indicate a good reproduction of the experimental data, aiding in the determination of the fuel flexibility of the burner.

Flame Characterization

The OH* chemiluminescence results for the steady state operating conditions (preheat air temperature of 873K) are presented below in Figures 4-6. Figure 4 depicts the flame shape and relative lift-off heights for AFER values ranging from 1.75 to 2.95 and lower heating values ranging from 7MJ/kg to 49MJ/kg at 80kW thermal power. Take note that the analyzed OH* image intensities are normalized to the individual image maximums, in order to more precisely describe the physical flame characteristics.

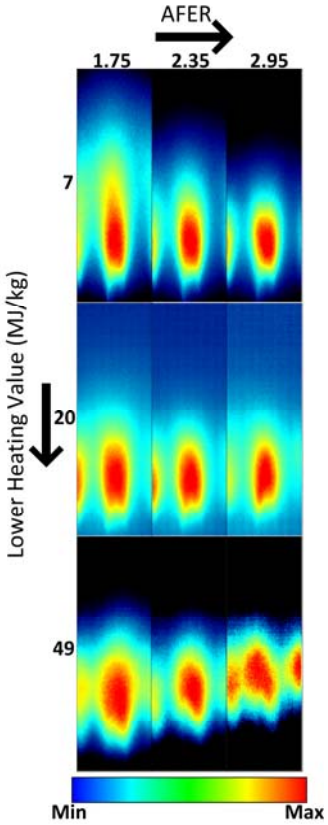

Figure 4 OH* Chemiluminescence Time Averaged Images for Varying Fuel Compositions and AFER Values at 80kW Thermal Power

As depicted in Figure 4, there are only small discrepancies in flame shape and lift-off height for varying AFER values and fuel compositions. Longer flame lengths

are apparent for lower AFER values and smaller lower heating values. The longest flame length is shown for the AFER 1.75-7MJ/kg test point, due to the richer fuel conditions and higher jet momentum at lower AFER values, as well as the increased hydrogen content at smaller lower heating values. The flames produced from only natural gas (49MJ/kg) display larger flame lift-off heights compared to the other fuel compositions tested, as displayed in Figure 5. The increase in lift-off height is due to a lack of hydrogen content in the fuel. Fuel mixtures with hydrogen present tend to sit directly above the burner, due to the increased reactivity of hydrogen. Additionally, it is apparent that the natural gas flames shift toward a more distributed flame zone at lower AFER values compared to mixtures containing syngas, as shown by the AFER 2.95-49MJ/kg test point in Figure 4. Although the images display small discrepancies in the flame characteristics over the ranges tested, overall the flames stabilize above the burner with a consistent flame shape and do not induce flashback or propagate large distances into the combustion chamber.

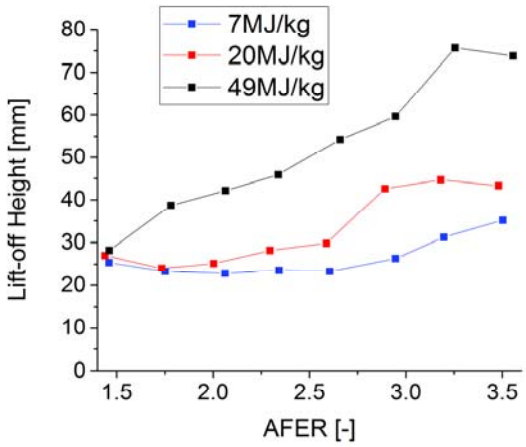

Figure 5 Lift-off Height vs. AFER for Varying Fuel Compositions and AFER Values at 80kW Thermal Power

The OH* chemiluminescence data also illustrates changes in intensity as the fuel compositions and power vary. Figure 6 shows the effects of the thermal power and lower heating value on the OH* intensity for thermal powers ranging from 60kW to 100kW and varying lower heating values ranging from 7MJ/kg to 49MJ/kg at an AFER of 2.35. Take note that the analyzed OH* image intensities are normalized to a constant global intensity in order to more accurately compare the OH* intensity characteristics of the corresponding test points.

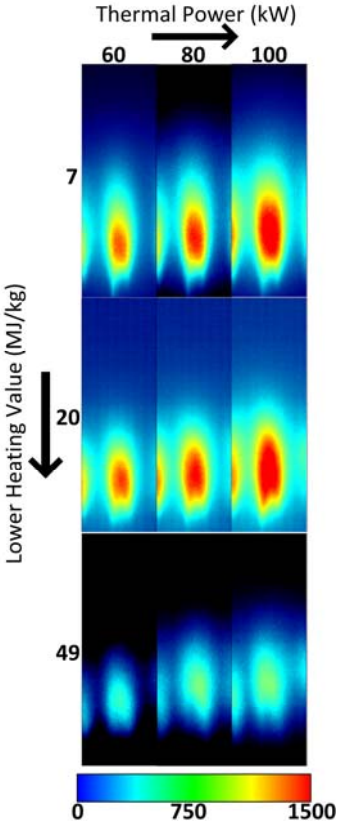

Figure 6 OH* Chemiluminescence Time Averaged Images for Varying Thermal Powers and LHVs at AFER 2.35

As displayed in Figure 6, the OH* intensity increases as the thermal power increases. This trend is due to the increased fuel content present at higher thermal loads, where increased fuel amounts, lead to a higher rate of combustion reactions, producing more intermediate OH* radicals for a given time period, ultimately increasing the OH* chemiluminescence signal. Additionally, as the lower heating value increases, the intensity decreases. This trend is due to the amount of hydrogen content present. As the lower heating value decreases, the hydrogen content in the fuel mixture increases, ultimately increasing the intermediate OH* radicals present for a given time period. This trend is displayed in the results above for AFER values above 1.0 (stoichiometric), whereas the opposite trend is described in literature for fuel-rich conditions (Garcia-Armingol and Bellester, 2014).

Emissions Results

Exhaust emissions data for the steady state operating conditions were also recorded and analyzed to determine the stability and functionality of the burner. Figure 7 depicts the CO and NO_x emissions vs the adiabatic flame temperature for the 7MJ/kg, 20MJ/kg and 49MJ/kg (shown as plots a), b) and c), respectively) fuel compositions.

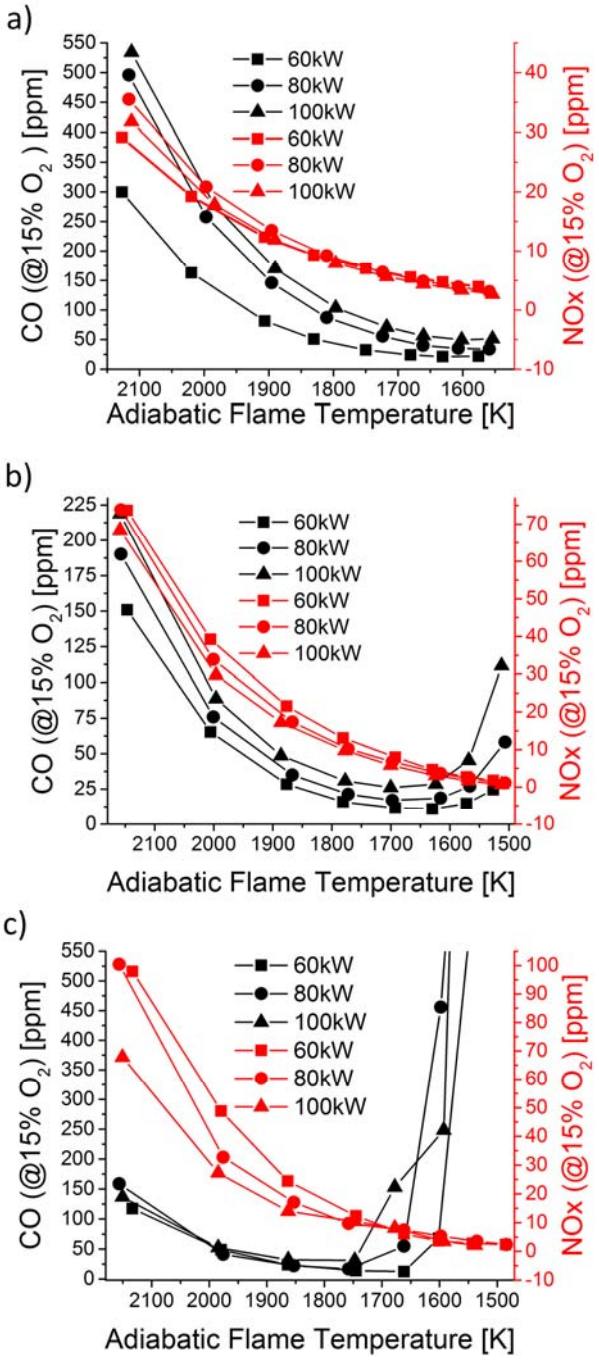

Figure 7 CO and NO_x Emissions vs Adiabatic Flame Temperature for a) 7MJ/kg, b) 20MJ/kg and c) 49MJ/kg

The CO and NO_x emissions levels display similar overall trends for all adiabatic flame temperatures and fuel compositions tested. The CO emissions depict a U-shaped trend. The left side of the U-shaped trend is clear in Figure 7 for the 7MJ/kg and 20MJ/kg plots. At higher adiabatic flame temperatures (moderately fuel-lean AFER values), large amounts of CO are produced from the dissociation of CO_2 (Lefebvre, 1983). The right side of the U-shaped trend displays increasing CO levels as the adiabatic flame temperature decreases (the AFER approaches the lean blow off limit). This is due to slow rates of oxidation from low combustion temperatures (Lefebvre, 1983).

The lean blow off limit also shifts to lower AFER values as the lower heating values increase. This is due to a decreased amount of hydrogen content in the fuel as the lower heating value increases. With less hydrogen, the combustion kinetics are slower, creating an unstable flame.

In addition, the NO_x levels decrease exponentially as the adiabatic flame temperature decreases, displaying NO_x concentrations less than 10ppm (normalized to 15% O_2) for all thermal loads and fuel compositions tested at adiabatic flame temperatures of 1700K and below. This trend is due to the suppression of thermal NO_x formation, based on the Zeldovich reaction mechanism (Baulch et al., 1994). Thermal NO_x formation has a direct dependence on the adiabatic flame temperature. Therefore, as the adiabatic flame temperatures decrease (AFER values increase), lower NO_x emissions levels result.

For the full range of fuel compositions and adiabatic flame temperatures tested, there is a weak influence of the thermal load on the NO_x and CO emissions. All thermal loads tested display similar trends, however lower thermal loads display lower emissions levels for the majority of adiabatic flame temperatures and thermal loads tested. Reduced flow rates at lower thermal powers enable larger residence times, causing the CO emissions levels to decrease (Zornek et al., 2013). NO_x emissions levels also decrease at lower thermal loads, due to the suppression of the four different NO_x formation pathways, as described in literature (Marnatz et al., 2006; Zornek et al., 2013).

As of 2016, the proposed German CO and NO_x emissions legal limits for gas turbines with an electrical power output less than 50MW are 80ppm and 37ppm for fuels excluding natural gas, respectively. For natural gas, the German legal limit remains at 80ppm for CO and is decreased to 24ppm for NO_x (German Federal Ministry for the Environment, 2016). Overall, based on the exhaust gas emissions data, adiabatic flame temperatures from 1550K to 1750K (AFER values 2.7 to 3.5) for the 7MJ/kg fuel composition yield exhaust gas emission levels below the proposed German legal limits, as displayed in Figure 7. Similarly, adiabatic flame temperatures from 1565K to 1875K (AFER values 2.0 to 3.2) and 1700K to 1860K (AFER values 2.0 to 2.5) for the 20MJ/kg and 49MJ/kg fuel compositions also yield exhaust gas emissions levels under the proposed German legal limits, respectively. Therefore, the adiabatic flame temperature (AFER) ranges listed above are considered the optimal burner operating ranges for the given fuel compositions. Since the MGT operating conditions are at a pressure ratio below five, it can be assumed the emissions levels at atmospheric conditions are comparable to that in a MGT system.

In MGT systems, dilution air is injected after the main reaction zone to decrease the combustor exit air temperature to a viable turbine operating temperature. In order to determine the actual optimal operating range of the burner in a MGT system, the dilution air needs to be taken into account. Figure 8 depicts the CO and NO_x emissions levels

vs. the air split (air through the combustor/total air in the system) for varying fuel compositions at 80kW thermal power (normal operating thermal power of the MGT). By increasing the air split, the adiabatic flame temperature is decreased (without taking the dilution air into account). Based on the information provided in Figure 8, air splits between 0.27 and 0.40 (vertical red lines in plot a)) display CO emissions levels below the proposed German legal limit (horizontal red line in plot a)) for all fuel compositions tested. Furthermore, air splits starting from 0.29 (vertical red line in plot b)), with no real upper limit, display NO_x emissions levels below the proposed German legal limit (horizontal red line in plot b)) for all compositions tested. Therefore, adequate MGT operational air splits for the tested burner are between 0.29 and 0.40.

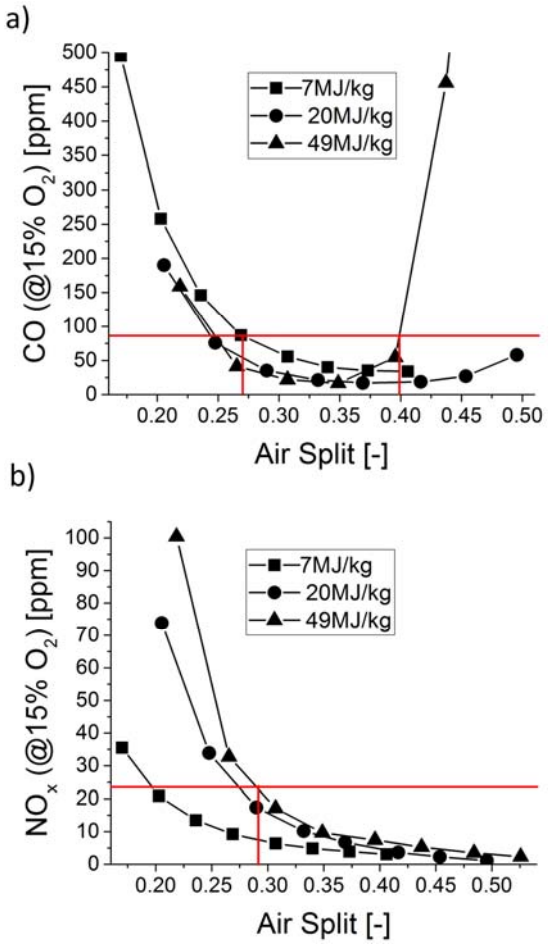

Figure 8 a) CO and b) NOx Emissions vs. Air Split for Varying Fuel Compositions at 80kW

CFD Simulation Results

First, the reaction zone shapes and lift-off heights between the simulations and experiments for both test cases (7MJ/kg and 49MJ/kg) at 80kW thermal power are compared. The comparison is made to justify using the CFD results to explain the flow field and combustion characteristics of the burner. Figure 9 displays the comparison between the experimental and simulated results for both test cases. As depicted and discussed in the previous subsection, the 49MJ/kg test points show larger flame lift-off heights compared to that of the 7MJ/kg points. This trend, which is captured well in the CFD, is due to higher flame speeds present at smaller lower heating values. Additionally, the mean simulation reaction shape profile indicates an inversed U-shape reaction zone. However, the simulations depict fewer reactions occurring at the flame centerline compared to the experimental results, which could be due to weaknesses in evaluating the mixing processes in the turbulence model, as well as a lack of transient effects in the steady-state simulation. Furthermore, spatial extensions of the mean reaction zones are also in good agreement, considering the computational and modelling effort of a steady state RANS simulation. Therefore, the numerical simulation results are in overall good agreement with the experimental results for the differing fuel compositions and thus, are employed to examine the flow field and temperature characteristics of the burner.

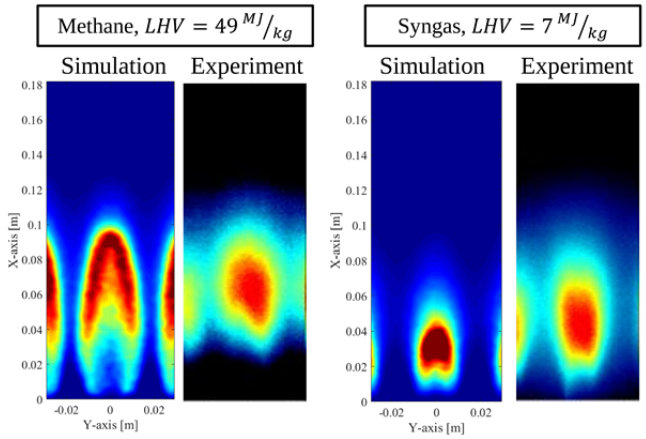

Figure 9 Qualitative Comparison between the Line-of-Sight Summarized CFD Heat Release and Integrated Experimental OH* Emission for the 7MJ/kg and 49MJ/kg Test Cases

Figure 10 displays the flow field and combustion characteristics of a cross section of the burner, featuring two jets (not through their respective centerline) issuing through the chamber. The partially premixed fuel/air jets display maximum velocities of approximately 90m/s in the axial direction for the 49MJ/kg test case (AFER of 2.35, 80kW). Furthermore, there are several separated recirculation zones, due to the interaction of the pilot stage with the main stage. The two large recirculation zones at the burner centerline axis have maximum negative velocities of approximately 45m/s. Additionally, there is an outer recirculation zone in the pilot stage, which has a maximum negative velocity slightly lower than that of the burner centerline recirculation zones. Furthermore, the largest main stage recirculation zone returns hot combustion products to the jet reaction zone and therefore, produces an additional stabilizing effect and creates relatively homogeneous temperature distributions in

the chamber, with peak temperatures at approximately 1850K.

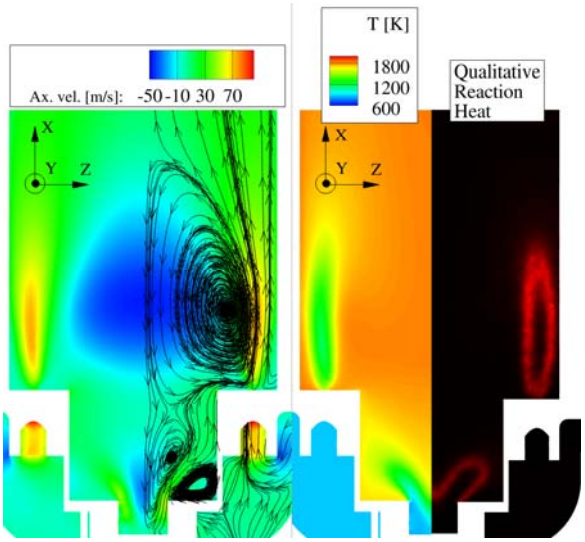

Figure 10 Flow Field and Combustion Characteristics from the CFD RANS Simulations for the 49MJ/kg Test Case

CONCLUSIONS

The stability and fuel flexibility of a ten nozzle, two-stage jet-stabilized burner has been studied and analyzed in an atmospheric test rig. Varying fuel compositions, consisting of natural gas, hydrogen, carbon monoxide, carbon dioxide and nitrogen, with lower heating values ranging from 7MJ/kg to 49MJ/kg have been tested. Flame stability and low emissions levels were presented for the majority of fuel compositions and thermal loads tested, therefore signifying high fuel flexibility of the burner. Only small discrepancies in the flame length and lift-off height were determined for all tested points, however larger lower heating values presented larger lift-off heights. Overall, the flames stabilized over the burner with a consistent flame shape and did not induce flashback or propagate large distances into the combustion chamber. Therefore, it is concluded that the burner is projected to function with varying fuel compositions, producing no significant instabilities when operated in the MGT.

The NO_x and CO emissions displayed similar trends for all fuel compositions and thermal loads tested. The CO emissions depicted a U-shaped trend, where the left and right sides of the U-shape were due to the dissociation of CO_2 and slow rates of oxidation from low combustion temperatures as the flame approaches the lean blow off limit, respectively. Additionally, the NO_x levels decreased exponentially as the AFER increased, for all thermal loads tested, due to a decrease in thermal NO_x formation as the adiabatic flame temperature decreased. Furthermore, air split ratios between 0.29 and 0.40 display CO and NO_x emissions levels below the proposed German legal limits for all fuel compositions tested. Therefore, the burner is projected to operate in a MGT within the legal German emissions limits, while still operating steadily and providing adequate power outputs.

Lastly, CFD RANS simulations were employed for the determination of the mean reaction zone positions and spatial extensions, providing good agreement with experimental results at low computational costs. The CFD results were then used to explain the flow field and combustion characteristics of the burner at selected operating conditions. The CFD simulations can therefore aid in further burner optimization and help predict burner performance in the MGT.

In conclusion, the results indicate a feasible, fuel flexible burner that can be implemented and further tested in MGT systems, using various natural gas and syngas fuel compositions. Furthermore, this study indicates the ability to shift from conventional to renewable fuel sources, while still utilizing existing infrastructure.

NOMENCLATURE

Greek

λ	Wavelength

Abbreviations

AFER	Air-Fuel Equivalence Ratio
CCD	Charged Coupled Device
CO	Carbon Monoxide
EDC	Eddy Dissipation Concept
FLOX®	Flameless Oxidation
IRO	Intensified Relay Optics
LHV	Lower Heating Value
LPC	Lean Premixed Condition
MGT	Micro Gas Turbine
NO_x	Nitrogen Oxides
OH*	Hydroxyl Radical
RANS	Reynolds Averaged Navier Stokes

ACKNOWLEDGMENTS

The authors wish to thank J. Zanger and T. Lingstädt for their support in the data acquisition, as well as F. Setzwein and M. Bentel for their help with the numerical simulation. Furthermore, the authors would like to thank the German Federal Ministry for Economic Affairs and Energy for the project funding.

REFERENCES

Asadullah M. (2014). Barriers of commercial power generation using biomass gasification gas: A review. Renewable and Sustainable Energy Reviews 29, 201-215. doi: 10.1016/j.rser.2013.08.074

Baulch D. L, Cobos C. J., et al. (1994). Evaluated Kinetic Data for Combustion Modeling - supplement I. Journal of Physical and Chemical Reference Data 23(6), 847 – 1033. doi: 10.1063/1.555953

Dahmen N., Henrich E., Dinjus E., Weirich F. (2012). The bioliq® bioslurry gasification process for the production of biosynfuels, organic chemicals, and energy. Journal of Energ, Sustainability and Society 2 (3). doi: 10.1186/2192-0567-2-3

Garcia-Armingol T. and Bellester J. (2014). Flame chemiluminescence in premixed combustion of hydrogen-

enriched fuels. International Journal of Hydrogen Energy 29 (21), 11299-11307. doi: 10.1016/j.ijhydene.2014.05.109

German Federal Ministry for the Environment (2002). Nature Conservation and Nuclear Safety. TA Luft. Available at http://www.bmu.de

German Federal Ministry for the Environment (2016). Nature Conservation and Nuclear Safety. TA Luft. Available at http://www.bmu.de

Gupta K.K., Rehman A., and Sarviya R.M. (2010). Bio-fuels for the gas turbine: A review. Renewable and Sustainable Energy Reviews 14 (9), 2946-2955. doi: 10.1016/j.rser.2010.07.025

Huang Y. and Yang V. (2009). Dynamics and stability of lean-premixed swirl-stabilized combustion. Progress in Energy and Combustion Science 35, 293-364. doi: 10.1016/j.pecs.2009.01.002

Kathrotia T. (2011). Reaction Kinetics Modeling of OH*, CH* and C2* Chemiluminescence. PhD thesis, Heidelberg University.

Kazakov A., and Frenklach M. (1994). Reduced reaction sets based on GRIMech1.2. Available at http://www.me.berkeley.edu/drm/.

Lefebvre A. W. (1983). Gas Turbine Combustion. New York: Hemisphere Publishing Corporation. ISBN 1-56032-673-5

Li J., Zhao Z., Kazakov A., Chaos M., Dryer F.L., and Scire Jr. J.J. (2007). A Comprehensive Kinetic Mechanism for CO, CH2O, and CH3OH Combustion, Int. J. Chem. Kinet. 39, 109-136. doi: 10.1002/kin.20218.

Lückerath R., Meier W., and Aigner M. (2007). FLOX® Combustion at High Pressure With Different Fuel Compositions. Proceedings of ASME Turbo Expo 2007: Power for Land, Sea, and Air. number: GT2007-27337

Pilavachi P.A. (2002). Mini- and micro-gas turbines for combined heat and power. Applied Thermal Engineering 22, 2003-2014. doi: 10.1016/S1359-4311(02)00132-1

Schütz H., Lückerath R., Kretschmer T., Noll B., and Aigner M. (2006). Analysis of the Pollutant Formation in the FLOX® Combustion. In proceedings of ASME Turbo Expo 2006: Power for Land, Sea, and Air. GT2006-91041

Spliethoff H. (2010). Power Generation from Solid Fuels. Berlin: Springer. ISBN 978-3-642-02856-4

Warnatz J., Maas U., and Dibble R.W. (2006). Combustion: Physical and Chemical Fundamentals, Modeling and Simulation, Experiments, Pollutant Formation. Berlin: Springer-Verlag.

Zanger J., Monz T., and Aigner M. (2015). Experimental investigation of the combustion characteristics of a double-staged Flox®-based combustor on an atmospheric and a micro gas turbine test rig. In proceedings of ASME Turbo Expo 2015: Turbine Technical Conference & Exposition. GT2015-42313

Zanger J., Widenhorn A., Monz T. and Aigner M. (2011). 25. Deutscher Flammentag, Karlsruhe, 259-264.

Zornek T., Monz T., and Aigner M. (2013). A Micro Gas Turbine Combustor for the use of Product Gases from Biomass Gasification. In Proceedings of the European Combustion Meeting 2013.

Zornek T., Monz T., and Aigner M. (2015). Performance anaylsis of the micro gas turbine Turbec T100 with a new FLOX-combustion system for low calorific fuels. Applied Energy 159, 276-284. doi: 10.1016/j.apenergy.2015.08.075